

# Small-angle X-ray scattering study of the ATP modulation of the structural features of the nucleotide binding domains of the CFTR in solution

Lauretta Galeno · Elena Galfrè · Oscar Moran

Received: 25 October 2010/Revised: 17 January 2011/Accepted: 14 February 2011/Published online: 22 March 2011  
© European Biophysical Societies' Association 2011

**Abstract** Nucleotide binding domains (NBD1 and NBD2) of the cystic fibrosis transmembrane conductance (CFTR), the defective protein in cystic fibrosis, are responsible for controlling the gating of the chloride channel and are the putative binding site for several candidate drugs in the disease treatment. We studied the structural properties of recombinant NBD1, NBD2, and an equimolar NBD1/NBD2 mixture in solution by small-angle X-ray scattering. We demonstrated that NBD1 or NBD2 alone have an overall structure similar to that observed for crystals. Application of 2 mM ATP induces a dimerization of NBD1 but does not modify the NBD2 monomeric conformation. An equimolar mixture of NBD1/NBD2 in solution shows a dimeric conformation, and the application of ATP to the solution causes a conformational change in the NBD1/NBD2 complex into a tight heterodimer. We hypothesize that a similar conformational change occurs *in situ* and that transition is part of the gating mechanism. To our knowledge, this is the first direct observation of a conformational change of the NBD1/NBD2 interaction by ATP. This information may be useful to understand the physiopathology of cystic fibrosis.

**Keywords** ABC transporter · Cystic fibrosis · Protein structure · Protein-protein interactions · X-ray scattering · CFTR · Nucleotide binding domain

**Electronic supplementary material** The online version of this article (doi:10.1007/s00249-011-0692-5) contains supplementary material, which is available to authorized users.

L. Galeno · E. Galfrè · O. Moran (✉)  
Istituto di Biofisica, Consiglio Nazionale delle Ricerche,  
Via De Marini, 6, 16149 Genoa, Italy  
e-mail: oscar.moran@cnr.it

## Introduction

Cystic fibrosis transmembrane conductance regulator (CFTR) is a chloride channel belonging to the ABC protein family. CFTR is activated by the PKA-dependent phosphorylation of a regulatory domain, and channel gating occurs upon the binding of ATP to the nucleotide binding domains (NBD1 and NBD2) (Gadsby et al. 2006). More than 1,600 different mutations of the gene coding for CFTR (<http://www.genet.sickkids.on.ca/cftr>) can lead to cystic fibrosis (CF), a lethal hereditary disease.

According to the currently accepted concepts, the channel gate opens upon the binding of two ATP molecules to NBD1 and NBD2. The binding would favor a “dimerization” of these domains, which, in turn, would lead to a conformational change to open the channel (Vergani et al. 2005). Evidence supporting this mechanism is based on functional measurements (Vergani et al. 2003, 2005) and cross-linking experiments (Mense et al. 2006) on site-directed mutant channels. On the other hand, several indications support the concept that, in the presence of nucleotides, recombinant NBD1 and NBD2 tend to dimerize (Lu and Pedersen 2000; Kidd et al. 2004). Moreover, we have proposed that most CFTR potentiators that are potential drugs for CF therapy bind in a site located in the interface between NBD1 and NBD2 (Moran et al. 2005; Zegarra-Moran et al. 2007). However, there are not yet direct structural data to confirm these theories. Very few data on the structure of CFTR are available, as is true for most integral membrane proteins. Low resolution structure of the whole CFTR has been obtained by electron microscopy-based image reconstruction and electron diffraction of bidimensional crystals (Rosenberg et al. 2004; Awayn et al. 2005; Mio et al. 2008). The most frequent CF mutation, dF508, is located in NBD1. For this reason an

important effort was made to solve the structure of this domain at atomic resolution (Thibodeau et al. 2005; Lewis et al. 2005).

The small-angle X-ray scattering (SAXS) technique was applied to study the molecular structure of recombinant NBDs in solution. Our results shows that ATP modulates the conformation of CFTR nucleotide binding domain, inducing a tight dimerization of NBD1 and the NBD1/NBD2 mixture. Dimerization was not observed for NBD2.

## Materials and methods

### Protein production

Recombinant NBD1 and NBD2 polypeptides were produced as inclusion bodies in *Escherichia coli*, purified by affinity and gel filtration chromatography, and successively refolded by dialysis. In brief, cDNA coding for the human CFTR domains NBD1 (from residue 394 to residue 672) or NBD2 (from residue 1,191 to residue 1,480) were sub-cloned into plasmid pT7; NBD1-cDNA was inserted between NdeI and HindIII sites, and NBD2-cDNA was inserted between NdeI and SalI. A hexa-histidine coding segment was included at the 3' terminus of the open reading frame in both constructs. Protein synthesis was induced in *E. coli* BL21 Rosetta strain (Stratagene, La Jolla, CA, USA) transformed with plasmid vectors pT7-NBD1 or pT7-NBD2 with 1 mM IPTG. After 3 h cells were pelleted, re-suspended in TRIS buffer, and subjected to lysis by sonication. Inclusion bodies were solubilized by incubation in a buffer containing 8 M urea.

Protein extract was bound in a nickel-affinity chromatography column (HisTrap HP Columns; GE Healthcare, Uppsala, Sweden), and successively eluted with 500 mM imidazole buffer. Imidazole was then removed with a desalting column (HiTrap, GE Healthcare) and the protein was subsequently purified by gel filtration in a Superdex 200 column (GE Healthcare). The chromatographic peaks were checked by SDS-polyacrylamide electrophoresis and processed by dialysis to refold the protein. Proteins were refolded by a three-step dialysis procedure: dialysis against (1) a PBS containing 4 M urea and 500 mM arginine; (2) PBS containing 500 mM arginine; (3) PBS without further additives (neither urea nor arginine). After dialysis, the correct refolding of proteins was checked by measuring the fluorescence spectrum for tryptophan (excitation 295 nm), and for the two polypeptides, NBD1 and NBD2, whose emission peak shifts from about 365 nm for the denatured state, to about 340 nm for the folded protein. A further control of the correct refolding of the proteins was obtained by circular dichroism (CD). CD spectra were recorded with a Jasco J500a spectropolarimeter. Spectra in the far-UV

region (198–258 nm) were signal-averaged by adding at least 10 scans, and the baseline was corrected by subtracting a spectrum for the buffer obtained in an identical manner. The secondary structure of the proteins was determined by CDPro (Sreerama and Woody 2004). Refolded proteins were then concentrated to about 2 mg/ml by ultrafiltration (Amicon Ultra-10 K, Millipore, Bedford, MA, USA) and frozen at  $-80^{\circ}\text{C}$  until use.

Except when indicated, all reagents were purchased from Sigma-Aldrich (St. Louis, MO, USA). All purification and refolding procedures were done at  $6-8^{\circ}\text{C}$ . A detailed procedure for protein production is described in the Electronic Supplementary Material.

### ATP binding

Nucleotide binding was determined from the quenching of protein-tryptophan fluorescence upon ATP binding to the refolded proteins (Qu et al. 1997). Samples containing 1.8 nM NBD1, NBD2, or NBD1/NBD2 mixture in 100 mM Tris-HCl, pH 8.0, 5 mM  $\text{MgCl}_2$ , and 1 mM DTT, at 0–800  $\mu\text{M}$  ATP concentration, were excited with monochromatic light at 295 nm. Uncorrected emission spectra were collected from 305 to 400 nm. The dissociation constant ( $K_d$ ) was calculated by nonlinear regression of the data according to the equation:

$$\Delta F = \frac{\Delta F_{\max} \times [L]}{K_d + [L]}$$

where  $\Delta F$  is the decrease in fluorescence and  $[L]$  is the concentration of ATP.

### SAXS data collection and processing

SAXS data were collected at the ID14-EH3 beam line of the European Synchrotron Radiation Facility (ESRF), Grenoble. The sample-detector distance of 1.83 m covered the range of momentum transfer  $0.1 < s < 3.6 \text{ nm}^{-1}$  [ $s = 4\pi \sin(\theta)/\lambda$ , where  $2\theta$  is the scattering angle and  $\lambda = 0.093 \text{ nm}$  is the X-ray wavelength; the optical path of the X-ray through the sample is about 1 mm]. Protein samples, containing NBD1 or NBD2 alone, or equimolar mixtures of NBD1 and NBD2, were prepared in 50 mM phosphate buffer (pH 8.0) with 1 mM DTT. When required, samples were supplemented with 2 mM ATP. Before use, proteins were cleared with a 0.45  $\mu\text{m}$  filter (Ultrafree-MC, Millipore), and concentrated by ultrafiltration with an Amicon membrane. Solutions with protein concentrations between 0.5 and 1.7 mg/ml (see Table 1) were measured at  $10^{\circ}\text{C}$ . For each sample, we collected 10 spectra of 30 s each, for a total of 5 min of acquisition. Average of scattering data from the buffer without protein, done before and after each sample measurement, was used

**Table 1** Structural parameters of the CFTR nucleotide binding domains in solution, obtained from SAXS experiments

	NBD1		NBD2		NBD1/NBD2	
	Control	2 mM ATP	Control	2 mM ATP	Control	2 mM ATP
MM (kDa)	32.2		33.6		64.7	
MM <sub>exp</sub> (kDa)	34.3	75.4	35.1	34.2	64.5	69.5
<i>c</i> (mg/ml)	0.81	0.8	0.55	0.54	1.68	1.66
<i>I</i> (0)	10,094	21,930	7,009	6,671	39,171	41,886
<i>R<sub>g</sub></i> (nm)	1.78	2.13	1.82	2.01	2.76	2.13
<i>V</i> (nm <sup>3</sup> )	35.5	24.0	33.0	29.6	46.8	25.2
<i>S</i> (nm <sup>2</sup> )	66.2	107.5	62.4	82.8	281.8	126.5
<i>D<sub>max</sub></i> (nm)	4.65	5.76	4.82	5.45	7.89	6.29
<i>Maxi</i> (nm)	2.2	2.7	2.2	2.2	2.8	2.7
<i>R<sub>g</sub></i> * (nm)	1.78	2.13	1.8	1.96	2.77	2.14

*MM* and *MM<sub>exp</sub>* are the molecular mass calculated from the amino acid sequence and from the experimental data, respectively. *MM<sub>exp</sub>* was calculated from the extrapolation of the Guinier plot to the origin, *I*(0), and the protein concentration, *c*, relative to the scattering of 4.5 mg/ml bovine serum albumin [*I*(0) = 1,078,000]. *R<sub>g</sub>* is the gyration radius estimated from the slope of the Guinier plot. The structure invariants, the molecular volume *V*, and the molecular surface *S* were estimated from *I*(0) and the extrapolation of *I*(*s*) for large *s* values, according to the Prod law (Feigin and Svergun 1987). The maximum length of the particle *D<sub>max</sub>* was estimated from the distance distribution function, *P*(*r*), with a maximum value at *Maxi* and an estimated gyration radius *R<sub>g</sub>*\* estimated from the function

to subtract the background. The comparison of the 10 successive 30 s exposures of the same protein solution indicated no changes in the scattering patterns, i.e., no measurable radiation damage to the protein samples. The data were normalized to the intensity of the transmitted beam, and the scattering of the buffer was subtracted. Data acquisition for each preparation (NBD1, NBD2, and NBD1/NBD2, without and with 2 mM ATP) was repeated three to four times using fresh samples. Successive acquisition data that did not present relevant differences were averaged.

The forward scattering *I*(0) and the radius of gyration *R<sub>g</sub>* were computed using the Guinier approximation for *sR<sub>g</sub>* < 1.3. The distance distribution function *P*(*r*) was calculated using the indirect Fourier transform method implemented in the program GNOM (Svergun 1992). It was calculated for the complete *I*(*s*) spectra, as *s* = 3.6 nm<sup>-1</sup>. *P*(*r*) represents the probability of finding a point within the observed particle at a distance, *r*, from a defined point of reference. To determine maximum protein dimensions (*D<sub>max</sub>*), the *P*(*r*) function was computed while constrained to zero at *r<sub>max</sub>*, where *r<sub>max</sub>* ranged from ~2*R<sub>g</sub>* to ~6*R<sub>g</sub>* in 0.01 nm increments and the *r<sub>max</sub>* yielded a plausible *P*(*r*)-defined *D<sub>max</sub>*. Sample molecular mass was estimated by comparing the extrapolated forward scattering *I*(0) to a reference solution made of bovine serum albumin (Mylonas and Svergun 2007).

#### Ab initio structure determination

Low-resolution models of the NBDs were reconstructed ab initio using the program DAMMIF (Svergun 1999; Franke and Svergun 2009). This program represents the

protein as an assembly of beads inside a spherical search volume of diameter *D<sub>max</sub>*. Starting from a random assembly, DAMMIF employs simulated annealing to build scattering equivalent models fitting the experimental data *I<sub>exp</sub>*(*s*) to minimize discrepancy:

$$\chi^2 = \frac{1}{N-1} \sum \left[ \frac{I_{\text{exp}}(s_j) - cI_{\text{calc}}(s_j)}{\sigma(s_j)} \right]^2$$

where *N* is the number of experimental points, *c* a scaling factor, and *I<sub>calc</sub>*(*s<sub>j</sub>*) and *σ*(*s<sub>j</sub>*) are the calculated intensity from the model and the experimental error at the momentum transfer *s<sub>j</sub>*, respectively. Ab initio reconstruction was repeated 10 times for each SAXS curve, and resulting models were aligned and averaged using the package DAMAVER (Volkov and Svergun 2003). First models were superposed with SUPCOMB (Volkov and Svergun 2003) and compared to find the most probable one and outliers. The agreement between models is expressed in terms of normalized space discrepancy (Kozin and Svergun 2001). The model with the lowest average NSD is considered the most probable one, those with the highest NSDs are considered outliers. The accepted models are then aligned to the most probable and an occupancy probability map is computed. Low occupancy and loosely connected atoms are removed from the occupancy probability map, and a compact average model is obtained.

Optimized models were superposed to the crystallographic structure of the human CFTR monomeric NBD1 or NBD2, or head-to-tail dimeric NBD1, and homology models for the NBD1/NBD2 assembly (Moran et al. 2005; Mornon et al. 2009). Superposition of high resolution structures was done with a correlation-based low resolution

docking implemented in the package SITUS (Wriggers and Chacón 2001; Wriggers 2010).

## Results

### Expression, folding, and purification of NBD1 and NBD2

Human CFTR NBD1 and NBD2 were expressed as inclusion bodies and were folded *in vitro* by three-step dialysis. To increase significantly the yield of refolding, the concentration of urea was gradually reduced, first from 8 to 4 M, and then completely removed. The presence of arginine in the dialysis solution resulted in a more reproducible yield of folded protein. In order to estimate the refolding yield, the final protein concentration and the concentration of the protein prior to the dialysis steps were compared by measuring the absorbance at 280 nm. Using this protocol, the final yield of refolding of NBD1 and NBD2 was between 70 and 75%. Interestingly, when an equimolar mixture of NBD1 and NBD2 was processed for refolding, the yield slightly increased to about 80%. Addition of 2 mM ATP during refolding further increased the yield to about 80–85%, but that was avoided since ATP-free proteins were used as control. The integrity of the proteins was controlled by SDS-polyacrylamide electrophoresis (Fig. 1a), and the quality of the refolding was checked by the position of the tryptophan peak fluorescence emission spectrum. Unfolded protein showed the maximum shifted to red as the fluorophore is exposed to a polar environment. After refolding, when tryptophan is accommodated in the hydrophobic core of the protein, the fluorescence peak shifts by 25 nm to left (Fig. 1b).

Far-UV CD spectra of the refolded preparation of NBD1, NBD2, and NBD1/NBD2 equimolar mixtures (Fig. 1c) revealed highly structured polypeptides that were very similar in solution (24%  $\alpha$ -helix and 25%  $\beta$ -sheet for NBD1; 20%  $\alpha$ -helix and 30%  $\beta$ -sheet for NBD2; 25%  $\alpha$ -helix and 23%  $\beta$ -sheet for the NBD1/NBD2 mixture). The finding of higher  $\beta$ -sheet and lower  $\alpha$ -helix contents in CFTR NBDs in solution is consistent with previous reports of the preparation of this recombinant protein (Hartman et al. 1992; Logan et al. 1994). However, CD spectra measured from the refolded proteins were not significantly different from those measured from NBD1 and NBD2 purified from the soluble fraction of the bacterial cytoplasm (data not shown). Therefore, most probably the dialysis procedure used to refold NBD1 and NBD2 solubilized from the inclusion bodies with urea may recover their native conformation.

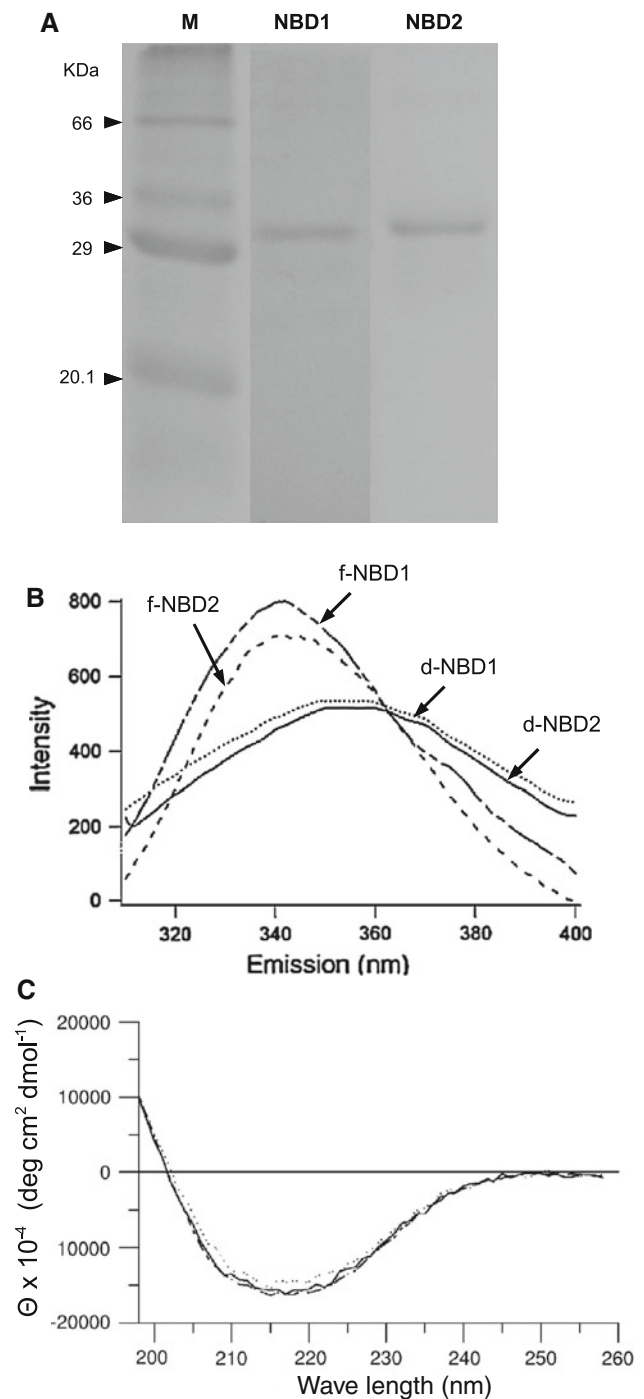


**Fig. 1a–c** Biochemical characterization of the recombinant NBD1 and NBD2. **a** SDS-polyacrylamide electrophoresis of the purified NBD1 and NBD2. *M* is the molecular mass markers lane, whose values are indicated on the left. **b** Fluorescence emission spectra of denatured (d-NBD1 and d-NBD2) and folded (f-NBD1 and f-NBD2) recombinant proteins. **c** CD-spectra were obtained from refolded and concentrated NBD1 (solid line), NBD2 (dotted line), and an isomolar mixture of NBD1 and NBD2 (broken line). Spectra were obtained at 20°C and in the absence of ATP

Gel filtration chromatography (Fig. 2a) supports that the three samples prepared are about mono-disperse, showing a single peak corresponding to a molecular mass of about 32 kDa for NBD1 and NBD2, while about twice that molecular mass was observed for more than 97% of the protein in the NBD1/NBD2 equimolar mixture chromatogram. These data also show that, even in the absence of ATP, the mixture of both NBDs tends to form a stable dimer, as previously observed using similar methods (Lu and Pedersen 2000).

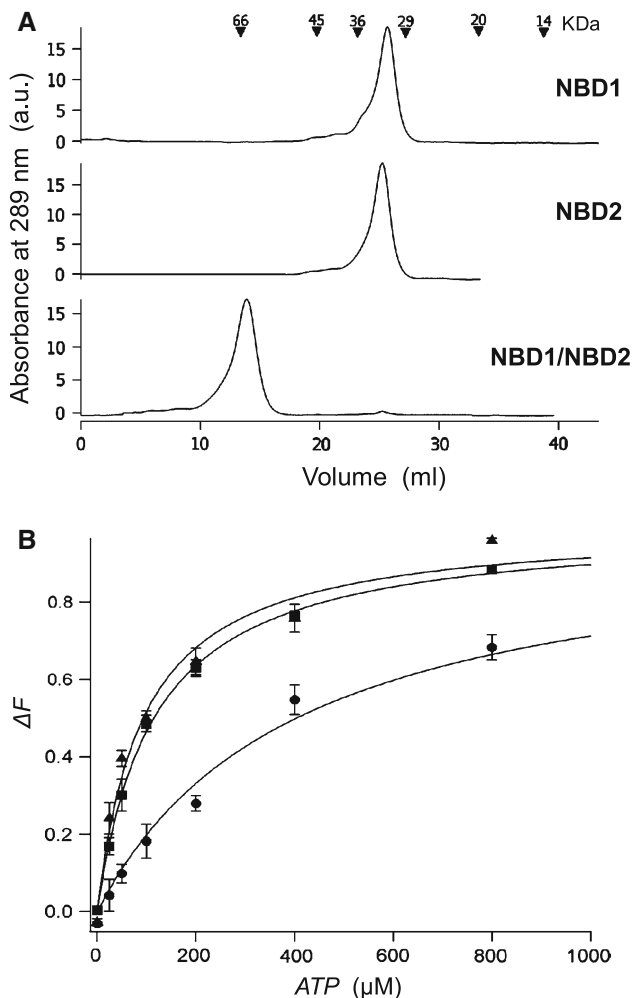


**Fig. 2a, b** Biochemical characterization of the recombinant NBD1 and NBD2. **a** Gel filtration chromatograms of the purified and refolded NBD1, NBD2, and NBD1/NBD2 mixture, as indicated, obtained in a Superdex 75 column (GE Healthcare). Chromatographic run was done at 7°C, using the same PBS as used for SAXS. Position of the peaks of calibration proteins and the corresponding molecular weight (bovine  $\alpha$ -lactalbumin 14.2 kDa, soybean trypsin inhibitor 20.1 kDa, bovine trypsinogen 24 kDa, bovine carbonic anhydrase 29 kDa, glyceraldehyde-3-phosphate dehydrogenase 36 kDa, egg albumin 44 kDa, bovine serum albumin 66 kDa) are shown at the top of the panel. **b** Langmuir isotherms for the ATP binding to NBD1 (squares), NBD2 (circles), and NBD1/NBD2 equimolar mixture (triangles). Bars are the standard errors from at least four experiments. The solid line is the least-squares fit with a rectangular hyperbola

The ability to bind ATP was checked to further test whether the proteins were correctly folded. The dissociation constants were  $115 \pm 3 \mu\text{M}$  for NBD1,  $403 \pm 31 \mu\text{M}$  for NBD2, and  $93 \pm 9 \mu\text{M}$  for the NBD1/NBD2 mixture (see Fig. 2b). Indeed, neither NBD1 nor NBD2, when denatured (in 8 M urea or 6 M guanidine chloride), showed a measurable ATP binding (data not shown).

Folded protein stability after freeze and thaw was a major problem encountered. About 30–40% of the protein undergoes aggregation after one freeze-thaw cycle. The aggregating fraction of NBDs could become even larger when the initial concentration is higher than 2 mg/ml. Therefore, frozen aliquots were always kept at concentrations below this limit, and, after thawing, samples were high-speed centrifuged (15,000g) and filtered before use for SAXS.

#### SAXS experiments on NBD1 and NBD2

The SAXS patterns from NBD1 and NBD2, after subtraction of the solvent scattering, are displayed in Fig. 3a, b, respectively. The extrapolation of the scattered intensity at  $s = 0$ ,  $I(0)$  (Fig. 3c, d, respectively), estimated from the Guinier plot of data (Guinier and Fournet 1955) yields an effective molecular mass of 34.3 kDa for NBD1 and 35.1 kDa for NBD2, which is compatible with the predicted value from the primary amino acid sequence (32.2 and 33.6 kDa for NBD1 and NBD2, respectively) by the SDS-polyacrylamide gel electrophoresis (Fig. 1a) and by gel filtration chromatography (Fig. 2a). This confirms that both NBD1 and NBD2 remain monomeric in solution under the experimental conditions used for carrying out the SAXS experiments. The gyration radii ( $R_g$ ) of NBD1 ( $1.77 \pm 0.02 \text{ nm}$ ) and NBD2 ( $1.82 \pm 0.02 \text{ nm}$ ) are very similar. These data are very similar to those measured from the crystallographic model of NBD1 (1.78–1.89 nm in 2BB0, 2PZE, and 2PZG) and the crystallographic model of NBD2 (1.82 nm for 3GD7). The Kratky plots of  $s^2I(s)$  versus  $s$  for the NBD1 and NBD2 data (Fig. 3a, b, inset) show bell-shaped curves typical of globular proteins (Glatter and Kratky 1982; Svergun and Koch 2003), indicating that both NBDs are rather compact in solution. The corresponding distance distribution functions  $P(r)$  for NBD1 and NBD2 are displayed in Fig. 3e, f, respectively. The  $R_g$  values calculated from the distance distribution function for both NBD1 and NBD2 were nearly identical to the one calculated with the Guinier plot. The maximum size of the proteins,  $D_{\text{max}}$ , for both domains is about 5 nm (see Table 1). The overall SAXS parameters thus suggest that NBD1 and NBD2 have a globular shape, which is also confirmed by the  $P(r)$  function, and have their maximum near  $D_{\text{max}}/2$  (Glatter and Kratky 1982).

The SAXS for the equimolar mixture of NBD1 and NBD2 is shown in Fig. 4a. Any attempt to adjust this

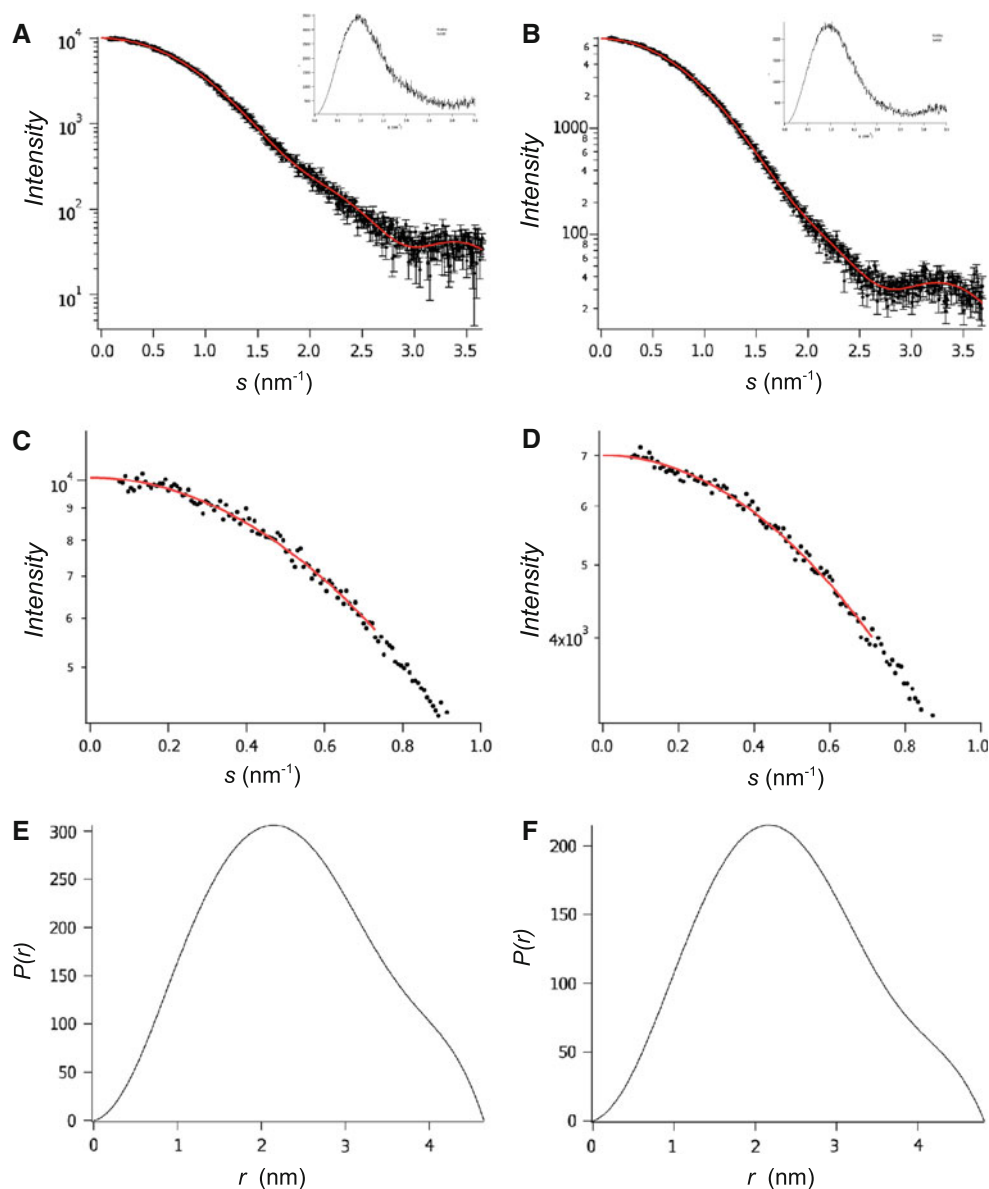


**Fig. 3a–f** SAXS data from CFTR NBD1 and NBD2 in the absence of ATP. SAXS patterns obtained from NBD1 (**a**) and NBD2 (**b**). Data represent the average intensity as a function of the momentum transfer,  $s$ , of three and four independent experiments, respectively. Bars are the standard deviations. The solid lines represent the reciprocal space fit of scattering computed for the final  $P(r)$  function

SAXS curve with a weighted sum of independent NBD1 and NBD2 SAXS patterns, assuming that it was produced by the mixture of independent NBD1 and NBD2 particles (Konarev et al. 2003), failed. The Guinier plot for the NBD1/NBD2 mixture SAXS pattern (Fig. 4b) rendered an  $I(0)$  corresponding to a molecular mass of 64.5 kDa, very close to the calculated summed mass of both domains (64.7 kDa), suggesting a dimer (NBD1/NBD2 dimer) was formed. This mass increase is consistent with the larger  $R_g$  ( $2.76 \pm 0.04$  nm) of the dimer. However, the value of  $R_g$  measured for the NBD1/NBD2 mixture, in the absence of

to data. The inset of each spectrum is the Kratky plot [ $s^2I(s)$  vs.  $s$ ]. The solid lines in **c** (NBD1) and **d** (NBD2) represent the extrapolation of data to  $s = 0$ , for  $sR_g < 1.3$  by the Guinier approximation. The corresponding distance distribution functions,  $P(r)$ , for NBD1 and NBD2 are represented in **e** and **f**, respectively

nucleotides, is bigger than estimated for the crystallographic data of the dimeric head-to-tail conformation of NBD1 (2PZE) or the homology models for the heterodimeric head-to-tail conformation of NBD1/NBD2 (Moran et al. 2005; Mornon et al. 2009), suggesting a possible different conformation. The shape of the  $P(r)$  for this sample (Fig. 4c) also shows a discrepancy towards a spherical form of the dimer. The maximum of  $P(r)$  is smaller than half of the value of  $D_{\max} = 7.89$  nm; moreover,  $P(r)$  shows a plateau or even has the aspect of a double peak, suggesting a shape consisting of two spherical

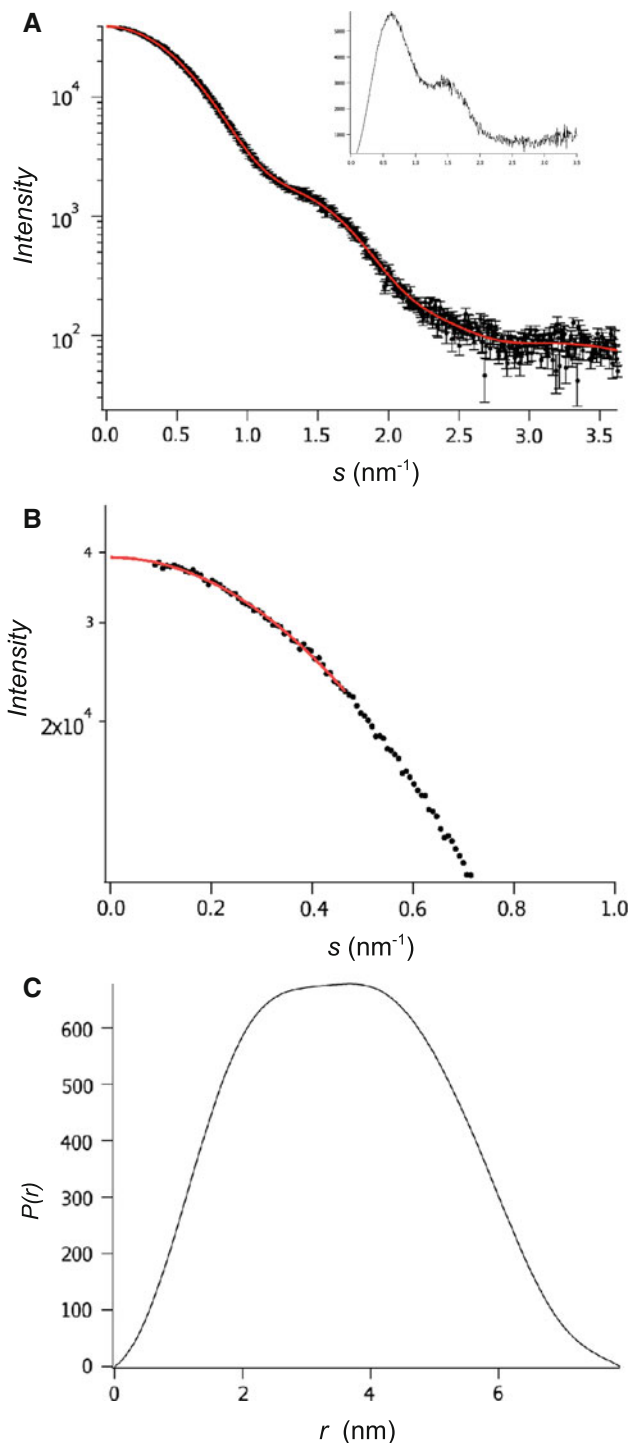


**Fig. 4a–c** SAXS data from an equimolar mixture of CFTR NBD1 and NBD2 in the absence of ATP. **a** SAXS patterns obtained from the NBD1/NBD2 mixture. Data represent the average intensity as a function of the momentum transfer,  $s$ , of four independent experiments. Bars are the standard deviations. The solid line represents the reciprocal space fit of scattering computed for final  $P(r)$  function to data. The inset is the Kratky plot [ $s^2 I(s)$  versus  $s$ ]. **b** The solid line is the extrapolation of data to  $s = 0$ , for  $sR_g < 1.3$  by the Guinier approximation. **c** The distance distribution function,  $P(r)$ , for the NBD1/NBD2 mixture

structures with a small separation between them (Svergun and Koch 2003). The Kratky plot for NBD1/NBD2 data also shows a bilobular shape, suggesting the presence of two subunits (see inset in Fig. 4a).

#### Low-resolution modelling of NBD1 and NBD2

Low-resolution models for NBD1, NBD2, and the NBD1/NBD2 dimer were generated by the ab initio program DAMMIF. The reconstruction of the three-dimensional form of the polypeptides was repeated 10 times for each construct. The model selection with the program DAMAVER discarded one of the low-resolution models of NBD1, and accepted all 10 models for NBD2 and the NBD1/NBD2 dimer. The average models of NBD1, NBD2, and the NBD1/NBD2 dimer in solution are displayed in Figs. 5a, b and 6, respectively.

The form reconstruction of NBD1 (Fig. 5a) and NBD2 (Fig. 5b), although slightly elongated, still shows a relatively compact shape in both polypeptides, with principal axis dimensions of  $4.8 \times 4.4 \times 4.3$  nm and  $5.3 \times 3.9 \times 3.8$  nm for NBD1 and NBD2, respectively. To confirm that the SAXS models obtained represent the polypeptides in solution, they were compared to the corresponding atomic structures (based on X-ray diffraction models) using SITUS. Three crystallographic models of NBD1 (2BBO and the two chains in 2PZG) were attempted to be docked into the volume defined by the low-resolution model. The docking procedure was run 10 times for each crystallographic structure, and a good convergence resulted for 5 docking possibilities for 2BBO, and for 6 and 5 docking results for chain A and chain B of 2PZG, respectively. The best correlation coefficient ( $R$ ) of docking ( $R = 0.851$ ), obtained with 2BBO, is presented in Fig. 5a, which shows that the crystalline structure of the human CFTR NBD1 is perfectly compatible with the low-resolution SAXS model of this polypeptide. Other murine NBD1 atomic structures reported (1ROW, 1ROY, 1ROZ) are also compatible as well with the SAXS model and are indistinguishable from the model presented in Fig. 5a (data not shown). Also the crystalline structure of NBD2 is compatible with the SAXS-based low resolution models. There, we attempted the docking of each of the four chains in 3GD7 to the low resolution model. The 10 docking trials for each chain converged to 3 models for chain A and 4 docking models for each chain B, C, and D. Figure 5b shows the best fitting obtained for the chain D of 3GD7 ( $R = 0.888$ ).

The low resolution reconstruction of the NBD1/NBD2 dimer resulted in an irregular form, which seems as if the NBD1 and NBD2 structures previously described are in contact at one extreme (Fig. 6), giving principal axis dimensions for the complex of  $7.0 \times 6.1 \times 6.1$  nm. We

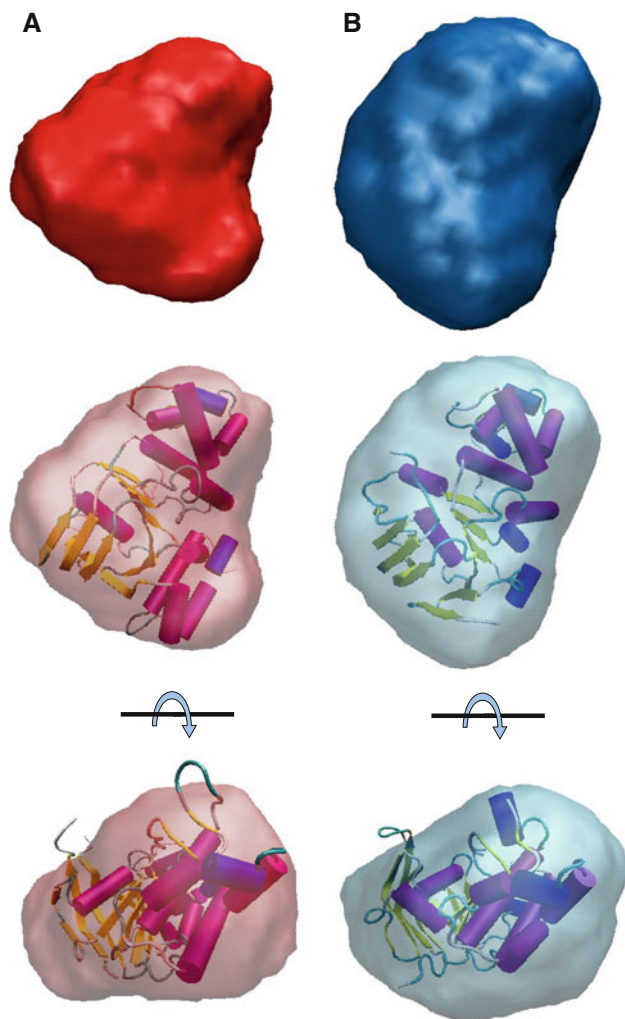


**Fig. 5a, b** Low resolution molecular models of NBDs in the absence of ATP. At the *top*, the ab initio rigid model of CFTR NBD1 (**a**) and NBD2 (**b**) in solution obtained using the program DAMMIF. In the *middle*, the semitransparent envelopes represent the same low resolution models, where the atomic structure of NBD1 (2BBO) and NBD2 (3GD7) have been docked, and at the *bottom*, the models have been rotated by 90° with respect to the horizontal axis

attempted to accommodate the atomic structure of the two domains, NBD1 and NBD2, inside the low resolution model. Figure 6 shows the best result of six simultaneous dockings of 2BBO (NBD1) and 3GD7, chain D (NBD2). The conformation is similar to that proposed for the closed state of the CFTR channel (Mornon et al. 2009).

#### ATP effects on NBDs conformation

The addition of 2 mM ATP to the solution containing NBD1 produced a significant modification of the geometrical and mass invariants of the sample. The extrapolation to the origin of the Guinier plot (Fig. 7b) yields a value of  $I(0)$  corresponding to a molecular mass of 75.4 kDa, about twice the mass of NBD1. Consistently,  $R_g$  was also

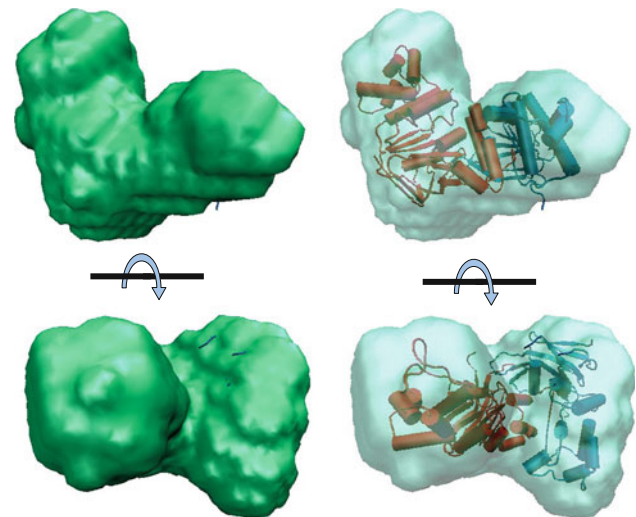


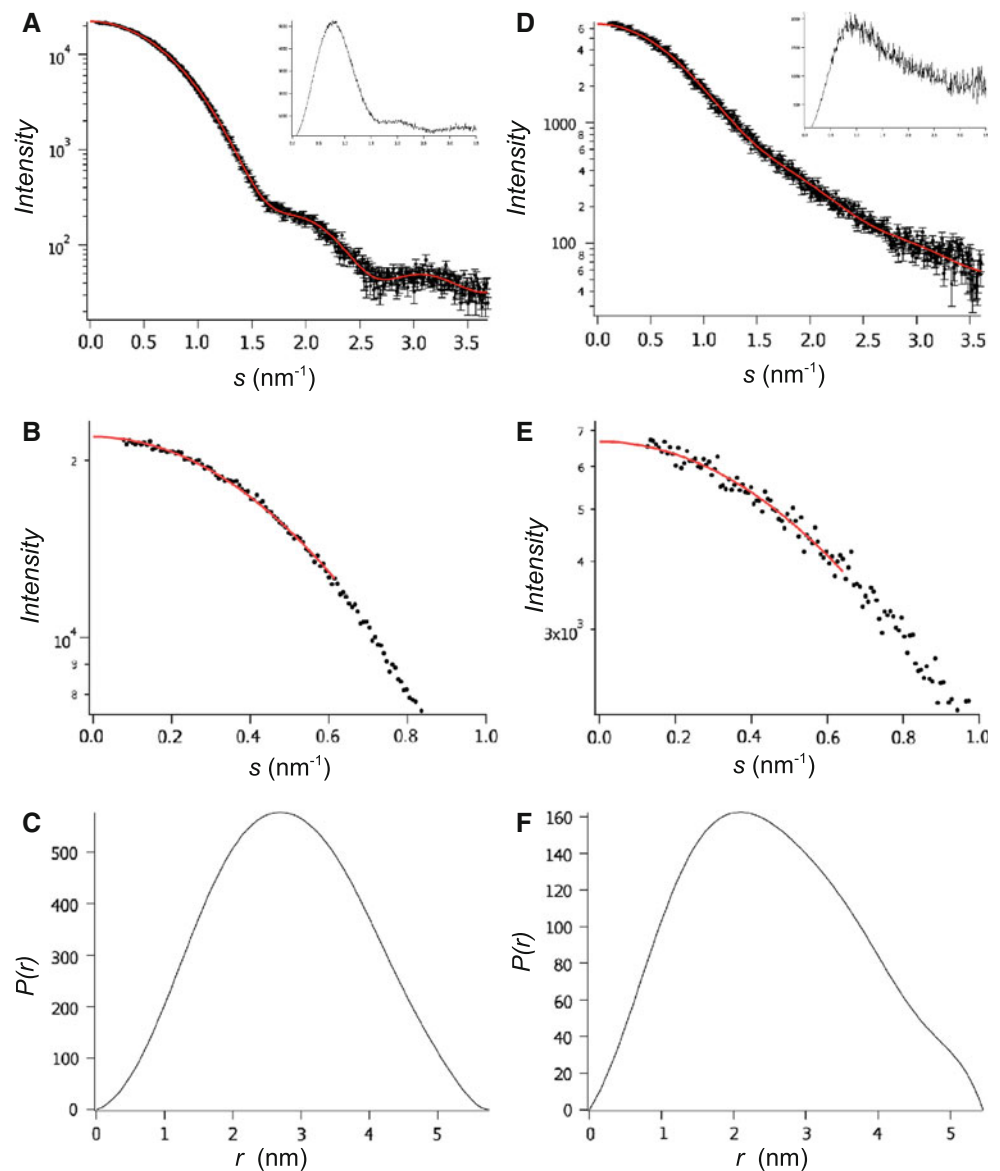
**Fig. 6** Low resolution molecular models of the equimolar mixture of NBD1 and NBD2 in the absence of ATP. The ab initio rigid model of CFTR NBD1/NBD2 in solution obtained using the program DAMMIF. The semitransparent envelopes represent the same low resolution models, where the atomic structure of NBD1 (2BBO) and NBD2 (3GD7) have been docked; the model, rotated by 90° with respect to the horizontal axis, is shown at the *bottom*

increased to 2.13 nm. This is similar to the value observed for NBD1 homo dimers (2PZG, 2.23 nm). The Kratky plot (Fig. 7a, inset) indicates that in the presence of ATP, NBD1 is a globular protein. This is in agreement with the  $R_g$  value estimated from the  $P(r)$  function (Fig. 7c), and is very similar to the one calculated with the Guinier plot, and to the maximum size of the proteins,  $D_{max}$ , of 5.76 nm, which is bigger than that measured for NBD1 in the absence of ATP (see Table 1).

Ab initio reconstruction of NBD1 in the presence of 2 mM ATP is shown in Fig. 8a. According to this model, the form of the molecule is about spherical, as suggested from the  $P(r)$  function, with principal axis dimensions of  $5.4 \times 5.2 \times 5.1$  nm. A single NBD1 molecule is not enough to fill this volume; it was necessary to use two NBD1 molecules to fit the model. Therefore, we attempted the docking of 2PZE, which represents the atomic model of CFTR NBD1 dimer in the head-to-tail configuration, into the volume defined by the SAXS-based model of NBD1 with 2 mM ATP. Figure 8a shows the best of the 4 docking models obtained after 10 docking runs. Similar results were obtained for the multiple docking of two molecules of NBD1, 2BBO, or 2PZG (data not shown).

Conversely, application of 2 mM ATP to NBD2 in solution does not significantly modify  $I(0)$  evaluated from the Guinier extrapolation (Fig. 7e), yielding an estimation of the molecular mass of 34.2 kDa, similar to the one estimated in the absence of ATP. The Kratky plot (Fig. 7d, inset) may reveal an increasing degree of disorder in the molecule, although a globular shape is maintained. The  $R_g$

**Fig. 7** SAXS data from CFTR NBD1 and NBD2 in a solution containing 2 mM ATP. SAXS patterns obtained from NBD1 (**a**) and NBD2 (**b**). Data represent the average intensity as a function of the momentum transfer,  $s$ , of four independent experiments, respectively. Bars are the standard deviations. The solid lines represent the reciprocal space fit of scattering computed for final  $P(r)$  function to data. The inset of each spectrum is the Kratky plot [ $s^2 I(s)$  versus  $s$ ]. The solid lines in **c** (NBD1) and **d** (NBD2) represent the extrapolation of data to  $s = 0$ , for  $sR_g < 1.3$  by the Guinier approximation. The corresponding distance distribution functions,  $P(r)$ , for NBD1 and NBD2 are represented in **e** and **f**, respectively



measured with the Guinier plot for NBD2 with ATP ( $2.01 \pm 0.02$  nm) is slightly larger than the one measured without ATP. The maximum size of the protein in the presence of ATP, evaluated from  $P(r)$  (Fig. 7f), is 5.45 nm, which is the maximum of the function in a position  $\langle D_{\max}/2$ , which reflects the slightly elongated shape of NBD2. Indeed, the ab initio modelling of the structure from the SAXS data yielded a globular, slightly elongated volume (Fig. 8b), with principal axis dimensions of  $5.2 \times 3.9 \times 3.8$  nm. Docking of the four chains reported in the crystallographic model of NBD2 on the low resolution model obtained in the presence of ATP resulted in a reasonable correlation coefficient, that was, however, lower than those obtained without ATP ( $R = 0.833$ ). These data confirm that the NBD2 subunit does not dimerize in the presence of 2 mM ATP.

The SAXS pattern obtained from the equimolar mixture of NBD1 and NBD2 in the presence of 2 mM ATP is shown in Fig. 9a. The scattering intensity extrapolation,  $I(0)$ , evaluated using the Guinier plot of the SAXS data (Fig. 9b) yielded an estimation of the molecular mass of 69.5 kDa. This is about the sum of the masses of the two components, NBD1 and NBD2, supporting the notion of a dimeric conformation of the mixture. Gel filtration chromatography of the equimolar NBD1/NBD2 mixture in the presence of ATP showed a single peak, corresponding to a molecular mass of  $\sim 69$  kDa, confirming the dimerization of the proteins (data not shown). The most probable composition of the dimer is a complex formed by one NBD1 and one NBD2. Other compositions would give different results. For example, we know that NBD2 does not form dimers in presence of ATP (see above). In the case of the

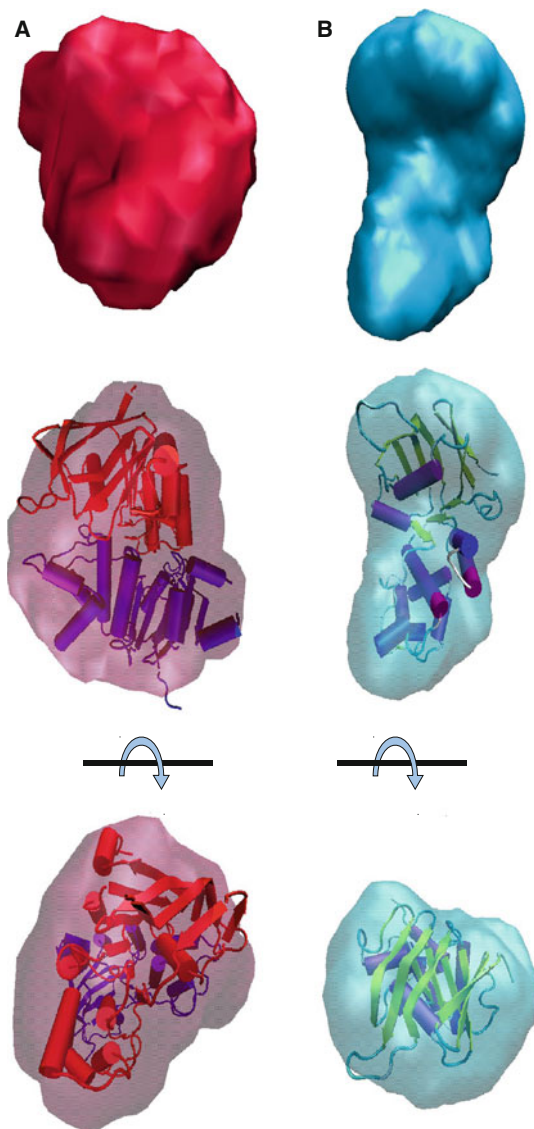


**Fig. 8a, b** Low resolution molecular models of NBDs from the SAXS data obtained in the presence of 2 mM ATP. At the *top*, the ab initio rigid model of the CFTR NBD1 (**a**) and NBD2 (**b**) in solution obtained using the program DAMMIF. In the *middle*, the semitransparent envelopes represent the same low resolution models, in which the atomic structure of the head-to-tail dimer of NBD1 (2PZE) and the NBD2 monomer (3GD7), respectively, have been docked. At the *bottom*, the models have been rotated by 90° with respect to the horizontal axis

formation of NBD1 homodimers, the SAXS data would be the sum of the spectra of NBD2 monomers and NBD1 dimers. Therefore, we attempted to fit the SAXS spectra with different hypotheses considering combinations of NBD1 monomers or homodimers and NBD2 monomers, with and without ATP, and the NBD1/NBD2 heterodimers without ATP. SAXS experimental data were fitted with these combinations of spectra in order to find the volume fractions of each component in the mixture with the

program OLIGOMER (Konarev et al. 2003). However, experimental data did not fit any of these hypotheses, leading us to conclude that the scattering was most probably produced by a NBD1/NBD2 heterodimer.

The structure of the NBD1/NBD2 dimer is a globular particle with an  $R_g$  of  $2.13 \pm 0.03$  nm, as measured with the Guiner plot. This is significantly smaller than the  $R_g$  evaluated in the absence of ATP. Hence, the dimer formed by NBD1 and NBD2 seems to compact in the presence of ATP, as suggested by the  $P(r)$  function presented in Fig. 9c, where the double peak observed in the data from the NBD1/NBD2 mixture in the absence of ATP in Fig. 4c was substituted by a single peak function, and  $D_{max}$  was reduced to 6.29 nm.

The ab initio model based on the SAXS data of the NBD1/NBD2 dimer in the presence of 2 mM ATP, which was a result of the average of the 10 runs of the program DAMMIF, yielded a spheroid with principal axis dimensions of  $5.2 \times 5.2 \times 5.1$  nm (Fig. 10a). As the atomic structure of NBD1/NBD2 has not been solved yet, we fitted the low resolution model of the dimer with the atomic model of the dimeric NBD1, 2PZE, or homology models of the NBD1/NBD2 dimer in the head-to-tail conformation (Moran et al. 2005; Mornon et al. 2009). This low resolution model could easily accommodate either the NBD1 dimer (Fig. 10b) or the model of the NBD1/NBD2 dimer (Fig. 10c).

## Discussion

The aim of this work was to study the molecular features of the human CFTR nucleotide binding domains. We expressed the isolated domains in bacteria and purified recombinant NBDs from inclusion bodies. The use of a denatured fraction of the protein has some advantages and some disadvantages. The main advantage is the big yield of the method compared to purifications of the protein from the soluble fraction of the cytoplasm. The disadvantage is that it is necessary to re-nature the protein to obtain a condition similar to the native protein. The most critical part of the procedure was, indeed, the refolding step. After trying several protocols, including dilution and other dialysis sequences, including variants with different additives to minimize the protein aggregation (see <http://refold.med.monash.edu.au/>), we found that the stepwise dialysis gave the most reproducible results. It is interesting to notice that the yield of the refolding procedure was increased when we dialysed an equimolar mixture of NBD1 and NBD2. The NBDs mixture spontaneously forms dimers, and probably this favors the folded conformation rather than the aggregated state.

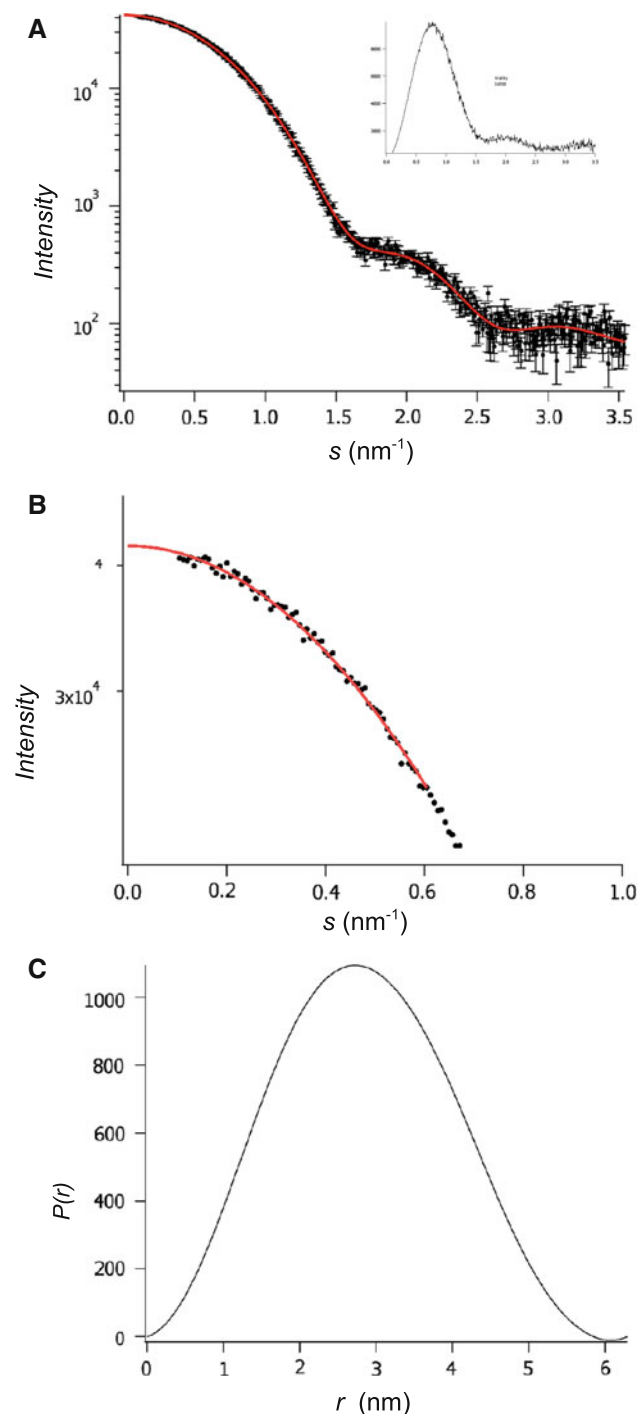


**Fig. 9a, b** SAXS data from an equimolar mixture of CFTR NBD1 and NBD2 in the presence of 2 mM ATP. **a** SAXS patterns obtained from NBD1/NBD2 mixture in the presence of ATP. Data represent the average intensity as a function of the momentum transfer,  $s$ , of five independent experiments. Bars are the standard deviations. The solid line represents the reciprocal space fit of scattering computed for final  $P(r)$  function to data. The inset is the Kratky plot [ $s^2 I(s)$  vs.  $s$ ]. **b** The solid lines are the extrapolation of data to  $s = 0$  for  $sR_g < 1.3$  by the Guinier approximation. **c** The distance distribution function,  $P(r)$ , for the NBD1/NBD2 mixture

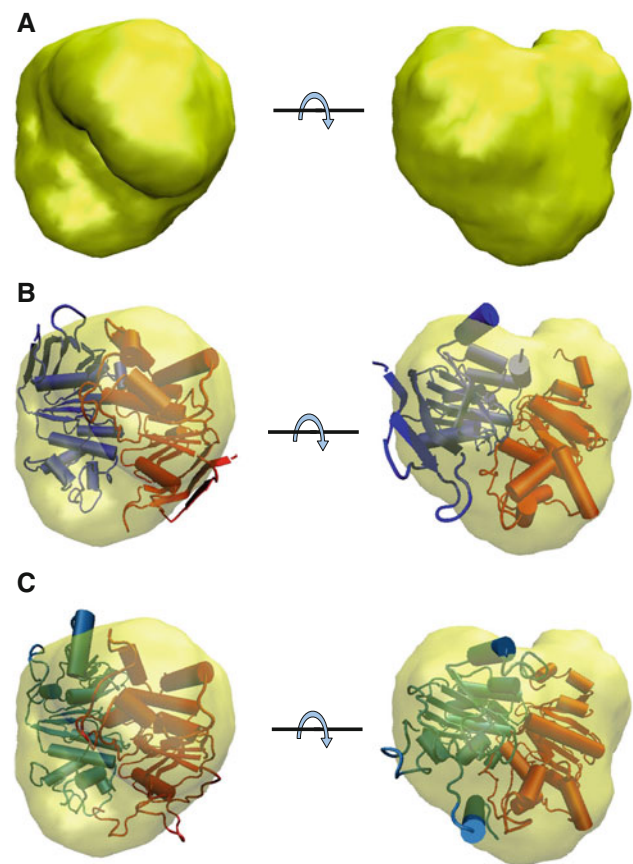


**Fig. 10a–c** Low resolution molecular models of the equimolar mixture of NBD1 and NBD2 in the presence of 2 mM ATP. **a** The ab initio rigid model of the CFTR NBD1/NBD2 in solution obtained using the program DAMMIF. **b** The semitransparent envelope represents the same low resolution model in which the atomic structure of the head-to-tail dimer of NBD1 dimer (2PZE) has been docked. **c** An NBD1/NBD2 homology model (Moran et al. 2005) was docked in the volume occupied by the low resolution SAXS model. Models, rotated by  $90^\circ$  with respect to the horizontal axis, are shown at right

We used several criteria to determine the quality of the refolded protein being used for SAXS experiments. First, we controlled that the fluorescence spectra for the refolded preparation corresponded to the native NBDs fluorescence spectra (Fig. 1b). We also measured the circular dichroism (CD) spectra of the refolded proteins (Fig. 1c). We noticed a difference between the secondary structure composition estimated by CD and values deduced from the crystallographic data of NBD1 and NBD2. This “excess” of  $\beta$ -sheets in CFTR NBDs in solution has been reported by other authors (Hartman et al. 1992; Logan et al. 1994; Karpowich et al. 2001). The same “excess” of  $\beta$ -sheets was also observed in CFTR NBDs purified from the soluble fraction of the bacteria (data not shown). It is interesting to observe that the secondary structure of the NBD of another

eukaryotic ABC protein, P-glycoprotein, has also been reported to contain a high fraction of  $\beta$ -sheets (>40%) and a low fraction of  $\alpha$ -helices (<15%) (Csanády et al. 2006), while the crystallographic data display different figures (31%  $\alpha$ -helix, 23%  $\beta$ -sheet; see PDB ID: 3G5U). We do not have any unequivocal explanation for the difference between the secondary structure determined from crystallographic data, although we could propose two hypotheses: first, analysis of CD data is not based on theoretical rigorous criteria but on a statistical comparison with other known structures by means a multi-parametric fit. Therefore, CD data interpretation does not yield absolute values but depends on the standard set and on the fitting criteria. The second hypothesis is that proteins in solution do not always have exactly the same secondary structure as observed in crystals. It is indeed interesting that most authors have reported similarly divergent data when analyzing NBDs in solution. Thus, one may have reservations regarding the identity of the molecular structure of these domains in solution and in situ in a real cell. Doubts may also arise with respect to the crystallographic model and the structure in situ.

As a further check of the preparation, we confirmed that the refolded proteins were able to bind ATP with equilibrium constants similar to those reported in the literature. From our preliminary data (not shown), we can also affirm that the refolded proteins are able to hydrolyze ATP with an enzymatic activity as follows: NBD1 < NBD2 < NBD1/NBD2.

We used this preparation to determine the properties of the molecular structure of the NBDs using the SAXS technique. The first observation is that both NBD1 and NBD2, when in solution, show a globular conformation with characteristic  $R_g$  that is consistent with those reported for the NBD1 and NBD2 atomic structures obtained by X-ray crystallography. Indeed, the *ab initio* reconstruction of the shape of these molecules from the SAXS data results in an envelope that can host the corresponding NBD1 or NBD2 crystallographic structure (Fig. 5). This result would support the concept that the crystalline structure of NBD1 is probably not too different from the structure of the NBDs in solution and vice versa. However, the question remains whether the conformation of these domains is similar in situ when they are integrated with other CFTR domains and probably form strong interactions with other regions of the protein.

Despite being homologous structures, different properties of NBD1 and NBD2 are revealed from their different responses to the application of ATP. In the presence of 2 mM of the nucleotide, NBD1 undergoes to a tight dimerization (Fig. 8a). Interestingly, this conformation is very similar to the crystallographic head-to-tail conformation reported for this subunit, as well as to the SAXS shape reconstruction of the NBD1/NBD2 dimer in the

presence of ATP. Instead, there was not evidence of a dimerization of NBD2 in 2 mM ATP, although a small conformational change could be observed (Fig. 8b), as supported by the lower correlation coefficient of the atomic NBD2 structure to the low density model. This difference could be caused by a relatively lower affinity of NBD2 for ATP. Considering their dissociation constants, we expect that more than 95% of NBD1 is ATP-bound at 2 mM concentration, but only 83% of NBD2 is nucleotide-bound. Assuming that binding of ATP is required and sufficient for the NBD2 dimerization, we would expect, in any case, a SAXS pattern that would be a linear combination of a dimeric (with a higher molecular mass) and a monomeric (as for the pattern obtained in absence of ATP) pattern of the NBD structure, weighted by the volume fraction of each component, in this case higher for the hypothetical NBD2 dimer. However, all attempts at interpreting the NBD2 data as a mixture of conformations, i.e., a weighted sum of two distinct patterns, did not give good results, and consequently we concluded that the presence of ATP does not induce a dimerization in NBD2.

The SAXS pattern obtained from the NBD1/NBD2 mixture in solution cannot be described as the addition of the properties of the single NBDs. Indeed, the geometric properties deduced from the data are compatible with the presence of a structure bigger than the simple NBD monomers, possibly a dimer. In the absence of ATP, the *ab initio* reconstruction of the NBD1/NBD2 dimer reveals a globular structure, with two divergent “wings” (Fig. 6). This shape is not compatible with the common head-to-tail conformation, such as that reported for NBD1 and the NBD1/NBD2 models (Moran et al. 2005; Mornon et al. 2009) or for the other ABC-protein NBDs. The best fit of this low resolution model with the atomic structures of NBD1 and NBD2 yields a conformation that has some analogies to the Mornon’s model of the conformation of the NBDs in the closed CFTR channel, based on homologies to bacterial proteins (Mornon et al. 2009). Indeed, the NBD1/NBD2 region of the Mornon’s model can be docked to the low resolution model of NBD1/NBD2 in the absence of ATP.

In the presence of 2 mM ATP, the NBD1/NBD2 dimer becomes tighter, and the  $R_g$  and the low resolution model obtained from the SAXS data are compatible with the expected head-to-tail conformation (Fig. 10). It may be noticed that this proposition, however, appears counterintuitive as NBD structures from all crystallographic studies of ABC proteins suggest that ATP has no access to the ATP binding site once a canonical NBD dimer has formed (Locher 2009). However, one must consider that this preparation is not a static preparation like a crystal, where the observed conformations may be constrained by the ordered crystalline interactions. Considering the equilibrium

constant of ATP and the NBD1/NBD2 dimer and the ATP concentration, we would have about 4% of dimer without ATP (not detectable with our method) in a conformation that is ready to bind the nucleotide. Probably, this binding induces the formation of more “canonical” dimers, but, at the same time, other dimers release the ATP (or the ADP hydrolysis product), maintaining the equilibrium of the system. The “compaction” of the NBD1/NBD2 dimer induced by ATP would be consistent with the “induced fit” mechanism proposed for bacterial ABC transporters (Neville et al. 1998; Annereau et al. 1997). However, not enough resolution could be attained by SAXS to unequivocally identify the singular regions of the domains involved in these conformational changes.

As mentioned before, the experimental conditions under which these data were obtained are different from the physiological conditions. Gating is very temperature sensitive, with bursts very much prolonged at lower temperatures, possibly correlated with a more stable NBD “compact” dimer (Sharma and Rose 1995), and these experiments were performed at 10°C. At this low temperature, the hydrolysis of ATP might be severely slowed, favoring the “compact” dimer configuration of NBD1/NBD2 in the presence of ATP. Further studies using different ATP concentrations and a higher temperature may be useful to investigate the role of the catalytic activity on the kinetics of conformational change of NBD1/NBD2.

We have to consider that these experiments were done with isolated domains in solution, while in the real CFTR the NBDs have several restrictions to their movement because of covalent and noncovalent interactions with other regions. It is tempting, however, to hypothesize that a similar conformation change occurs in situ and that transition is part of the gating mechanism (Vergani et al. 2005). Therefore, this is the first direct observation of the conformational change of the NBD1/NBD2 produced by ATP binding, perhaps a tight dimer formation.

In conclusion, we have studied the molecular features of the human CFTR in solution, demonstrating that NBD1 and NBD2 alone have a monomeric globular conformation, while the equimolar mixture of NBD1/NBD2 has a dimeric conformation. Application of ATP to the solution induces the dimerization of NBD1 and causes the NBD1/NBD2 complex to tighten, while NBD2 only marginally changes conformation, leaving it monomeric. It is interesting to notice that these results indicate that ATP would not induce the “dimerization” of NBD1 and NBD2, but a relatively small conformational change in the relative positions of CFTR NBD1 and NBD2 would be correlated with the channel gating (Vergani et al. 2005). These observations, together with those eventually implemented using CFTR potentiators or with CF-related NBD mutants, may be useful for the improvement of the pharmacological therapy

of CF and for the better understanding of the CF physiopathology.

**Acknowledgments** We thank the ESRF for provision of synchrotron radiation facilities, and we would like to thank Petra Pernod for assistance in using beamline ID14-EH3. We thank Olga Zegarra, Gino Galletta, Paola Vergani, and Ilaria Zanardi for their comments. This project was supported by the Fondazione Ricerca Fibrosi Cistica (grant #2/2008), Mille bambini a Via Margutta–onlus, Blunotte and Lega Italiana FC–Associazione Toscana Onlus.

## References

- Annereau JP, Wulbrand U, Vankeerberghen A, Cuppens H, Bontems F, Tümmler B, Cassiman JJ, Stoven V (1997) A novel model for the first nucleotide binding domain of the cystic fibrosis transmembrane conductance regulator. *FEBS Lett* 407:303–308
- Awaryn NH, Rosenberg MF, Kamis AB, Aleksandrov LA, Riordan JR, Ford RC (2005) Crystallographic and single-particle analyses of native- and nucleotide-bound forms of the cystic fibrosis transmembrane conductance regulator (CFTR) protein. *Biochem Soc Trans* 33:996–999
- Csanády L, Nairn AC, Gadsby DC (2006) Thermodynamics of CFTR channel gating: a spreading conformational change initiates an irreversible gating cycle. *J Gen Physiol* 128:523–533
- Feigin LA, Svergun DI (1987) Structure analysis by small-angle X-ray and neutron scattering. Plenum Press, New York
- Franke D, Svergun DI (2009) DAMMIF, a program for rapid ab initio shape determination in small-angle scattering. *J Appl Cryst* 42:342–346
- Gadsby DC, Vergani P, Csanády L (2006) The ABC protein turned chloride channel whose failure causes cystic fibrosis. *Nature* 440:477–483
- Glatter O, Kratky O (1982) Small angle X-ray scattering. Academic Press, London
- Guinier A, Fournet G (1955) Small angle scattering of X-rays. Wiley, New York
- Hartman J, Huang Z, Rado TA, Peng S, Jilling T, Muccio DD, Sorscher EJ (1992) Recombinant synthesis, purification, and nucleotide binding characteristics of the first nucleotide binding domain of the cystic fibrosis gene product. *J Biol Chem* 267:6455–6458
- Karpowich N, Martsinkevich O, Millen L, Yuan YR, Dai PL, MacVey K, Thomas PJ, Hunt JF (2001) Crystal structures of the MJ1267 ATP binding cassette reveal an induced-fit effect at the ATPase active site of an ABC transporter. *Structure* 9:571–586
- Kidd JF, Ramjeesingh M, Stratford F, Huan LJ, Bear CE (2004) A heteromeric complex of the two nucleotide binding domains of cystic fibrosis transmembrane conductance regulator (CFTR) mediates ATPase activity. *J Biol Chem* 279:41664–41669
- Konarev P, Volkov VV, Sokolova AV, Koch MHJ, Svergun DI (2003) PRIMUS: a Windows PC-based system for small-angle scattering data analysis. *J Appl Cryst* 36:1277–1282
- Kozin MB, Svergun DI (2001) Automated matching of high- and low-resolution structural models. *J Appl Cryst* 34:33–41
- Lewis HA, Zhao X, Wang C, Sauder JM, Rooney I, Noland BW, Lorimer D, Kearins MC, Connors K, Condon B, Maloney PC, Guggino WB, Hunt JF, Emtage S (2005) Impact of the DeltaF508 mutation in first nucleotide-binding domain of human cystic fibrosis transmembrane conductance regulator on domain folding and structure. *J Biol Chem* 280:1346–1353
- Locher KP (2009) Structure and mechanism of ATP-binding cassette transporters. *Philos Trans R Soc Lond B Biol Sci* 364:239–245

- Logan J, Hiestand D, Daram P, Huang Z, Muccio DD, Hartman J, Haley B, Cook WJ, Sorscher EJ (1994) Cystic fibrosis transmembrane conductance regulator mutations that disrupt nucleotide binding. *J Clin Invest* 94:228–236
- Lu NT, Pedersen PL (2000) Cystic fibrosis transmembrane conductance regulator: the purified NBF1+R protein interacts with the purified NBF2 domain to form a stable NBF1+R/NBF2 complex while inducing a conformational change transmitted to the C-terminal region. *Arch Biochem Biophys* 375:7–20
- Mense M, Vergani P, White DM, Altberg G, Nairn AC, Gadsby DC (2006) In vivo phosphorylation of CFTR promotes formation of a nucleotide-binding domain heterodimer. *EMBO J* 25:4728–4739
- Mio K, Ogura T, Mio M, Shimizu H, Hwang T, Sato C, Sohma Y (2008) Three-dimensional reconstruction of human cystic fibrosis transmembrane conductance regulator chloride channel revealed an ellipsoidal structure with orifices beneath the putative transmembrane domain. *J Biol Chem* 283:30300–30310
- Moran O, Galiotta LJV, Zegarra-Moran O (2005) Binding site of activators of the cystic fibrosis transmembrane conductance regulator in the nucleotide binding domains. *Cell Mol Life Sci* 62:446–460
- Momon J, Lehn P, Callebaut I (2009) Molecular models of the open and closed states of the whole human CFTR protein. *Cell Mol Life Sci* 66:3469–3486
- Mylonas E, Svergun DI (2007) Accuracy of molecular mass determination of proteins in solution by small-angle X-ray scattering. *J Appl Cryst* 40:s245–s249
- Neville DC, Rozanas CR, Tulk BM, Townsend RR, Verkman AS (1998) Expression and characterization of the NBD1-R domain region of CFTR: evidence for subunit-subunit interactions. *Biochemistry* 37:2401–2409
- Qu BH, Strickland EH, Thomas PJ (1997) Localization and suppression of a kinetic defect in cystic fibrosis transmembrane conductance regulator folding. *J Biol Chem* 272:15739–15744
- Rosenberg MF, Kamis AB, Aleksandrov LA, Ford RC, Riordan JR (2004) Purification and crystallization of the cystic fibrosis transmembrane conductance regulator (CFTR). *J Biol Chem* 279:39051–39057
- Sharma S, Rose DR (1995) Cloning, overexpression, purification, and characterization of the carboxyl-terminal nucleotide binding domain of P-glycoprotein. *J Biol Chem* 270:14085–14093
- Sreerama N, Woody RW (2004) Computation and analysis of protein circular dichroism spectra. *Methods Enzymol* 383:318–351
- Svergun DI (1992) Determination of the regularization parameter in indirect-transform methods using perceptual criteria. *J Appl Cryst* 25:495–503
- Svergun DI (1999) Restoring low resolution structure of biological macromolecules from solution scattering using simulated annealing. *Biophys J* 76:2879–2886
- Svergun DI, Koch MH (2003) Small-angle scattering studies of biological macromolecules in solution. *Rep Prog Phys* 66:1735–1782
- Thibodeau PH, Brautigam CA, Machius M, Thomas PJ (2005) Side chain and backbone contributions of Phe508 to CFTR folding. *Nat Struct Mol Biol* 12:10–16
- Vergani P, Nairn AC, Gadsby DC (2003) On the mechanism of MgATP-dependent gating of CFTR Cl<sup>-</sup> channels. *J Gen Physiol* 121:17–36
- Vergani P, Basso C, Mense M, Nairn AC, Gadsby DC (2005) Control of the CFTR channel's gates. *Biochem Soc Trans* 33:1003–1007
- Volkov V, Svergun D (2003) Uniqueness of ab initio shape determination in small-angle scattering. *J Appl Cryst* 36:860–864
- Wriggers W (2010) Using Situs for the integration of multi-resolution structures. *Biophys Rev* 2:21–27
- Wriggers W, Chacón P (2001) Using situs for the registration of protein structures with low-resolution bead models from X-ray solution scattering. *J Appl Cryst* 34:773–776
- Zegarra-Moran O, Monteverde M, Galiotta LJV, Moran O (2007) Functional analysis of mutations in the putative binding site for cystic fibrosis transmembrane conductance regulator potentiators. Interaction between activation and inhibition. *J Biol Chem* 282:9098–9104